actuators

Article

Practical and Rapid Motor Sizing Technique Using Existing Electrical Motor

Yong-Chul Kim [1], Jung-Ho Han [2] and Ju Lee [1,*]

[1] Department of Electrical Engineering, Hanyang University, 222, Wangsimri-ro, Seongdong-gu, Seoul 04763, Republic of Korea; yckimd@lginnotek.com
[2] LG Innotek, 111, Jinwi2sandan-ro, Jinwi-myeon, Pyeongtaek-si 17708, Republic of Korea
* Correspondence: julee@hanyang.ac.kr

Abstract: Electrical motor design requires considerable work and resources. In the field, motor designers need to decide on competitive motor sizing quickly to compete with other motor suppliers. Generally, expensive FEM S/W is required to obtain accurate motor sizing results, but buying and maintaining many licenses is costly. Moreover, patience is required to obtain the results from FEM analysis. In this paper, a motor sizing technique using an existing production motor is presented to enable responding to urgent requests from customers without using FEM analysis. In order to enhance the fidelity of the results, magnetic flux losses due to magnet coatings and non-linear characteristics are considered during the motor sizing process. The proposed sizing method is verified via a comparison with FEM analysis and the test results and shows reasonable performance. Also, this method has the substantial advantage of outputting accurate results instantly. The method can help with the modification design of electrical motors without using expensive FEM S/W and does not require a certain level of skill or experience.

Keywords: permanent magnet synchronous motor (PMSM); motor sizing; finite element method (FEM); electric power steering motor (EPS motor); magnetic flux loss; parameter; torque ripple; torque–speed

Citation: Kim, Y.-C.; Han, J.-H.; Lee, J. Practical and Rapid Motor Sizing Technique Using Existing Electrical Motor. *Actuators* **2023**, *12*, 430. https://doi.org/10.3390/act12120430

Academic Editors: Efren Diez-Jimenez and Ignacio Valiente Blanco

Received: 8 October 2023
Revised: 2 November 2023
Accepted: 17 November 2023
Published: 21 November 2023

1. Introduction

Permanent magnet synchronous motors have been used in various applications for centuries due to their many advantages, such as high efficiency, high torque-to-current and torque-to-volume ratios, compact structure, and fast dynamic response [1–11].

In particular, due to the global movement to reduce greenhouse gases, electrification is rapidly occurring in the automotive area. As a result, the adoption of electric motors to replace internal combustion engines and hydraulics, which are existing power sources, is increasing. Additionally, high-output and compact-size electric motors are required to improve vehicle efficiency [2,7,10,12].

Moreover, as suggested by Moore's Law, computer performance has improved dramatically, and as a result, the calculation speed of FEM S/W required for electric motor design and analysis has also improved dramatically. Therefore, multiple design models can be calculated more quickly and various system phenomena can be solved using software such as finite element analysis tools [13]. However, many commercial tools are expensive to purchase and maintain, making owning and maintaining many licenses burdensome unless the company or research institute is well funded. Therefore, in most cases, it is difficult for motor design engineers to use commercial software simultaneously with limited licenses, so it is necessary to establish a way to operate it efficiently.

In the field, motor design engineers are frequently asked by their customers to design and quote for electric motors that meet the desired performance within a short period of time. In the case of an expert with enough experience or lots of evaluated data and design references, there may be no risk in responding to such requests. However, it would be challenging work under time constraints in most cases. In addition, price competition among motor manufacturers is intensifying due to the extension of electric motor adoption to many applications. Furthermore, the market price needs to decrease gradually, making it more difficult to make a profit. In this case, most motor manufacturers can convert existing electric motors into a platform to increase production and lower manufacturing costs. This method can significantly reduce new investments via the manufacture of key components, such as the rotor and stator core, using the same tooling used to produce conventional products, changing the stack lengths and windings in different ways to meet the required performance. Additionally, the development period can be shortened, minimizing the resources required for development.

Nevertheless, as mentioned earlier, it is often impossible to use expensive motor design S/W promptly to respond to the tight timescales given by customers for electric motor design.

Therefore, in this paper, an effective motor sizing method that can be used in the field is proposed to solve this problem. To this end, a reference model to be used as a platform design was selected first and the evaluation and analysis data were collected via FEM for this motor as the reference data.

Then, the relationship between the wire diameter, number of turns, and lamination length, which are the design variables used when determining motor size, was derived for the fundamental parameters of the motor, such as resistance (*Rs*), inductance (*Ls*), and back EMF constant (*Ke*).

In order to increase the accuracy of calculations, the torque under load, torque ripple, and demagnetization characteristics of permanent magnets, which are nonlinear characteristics that change with the increase in the ampere-turn condition, were databased within the sizing process template by performing FEM analysis on the reference model. This process only needs to be performed once for the reference model, as there is no need to analyze it using expensive FEM S/W every time motor sizing is needed in the future. In this way, using the results in the database of the preformed template and the relationship between the three design variables (wire diameter, number of turns, and stacking length) and the motor performance, the characteristics of the motor can be quickly calculated and specifications that meet the relevant requirements can be found effectively in seconds.

In summary, the sizing method proposed in this paper has the substantial advantage of enabling the rapid design of an electric motor that meets the relevant requirements, regardless of the designer's experience and skill level, without using expensive S/W.

The motor sizing technique presented in this paper was first verified by comparing it with the FEM calculation results. Then, prototype samples were built and tested to verify the method's effectiveness.

2. Description of Analysis Model

The reference model to be used in this paper is a permanent magnet synchronous motor (PMSM) designed for automotive electric power steering systems, of which its configuration is shown in Figure 1. Since the steering system requires an electric motor with low cogging and ripple torque [2,6–9,14–17], the surface permanent magnet synchronous motor (SPMSM), with a skew in the stator or rotor, is mainly used, and this model has a three-step skewed rotor [15]. The main parameters for the reference model used in the sizing calculation in this paper are shown in Table 1, where these are the results of verifying consistency via a comparison of the test and analysis values.

Figure 2 shows the three design variables that are used in the design described in this paper, which are wire diameter, turns, and stack length.

Table 1. Motor parameters for design base model.

Parameters	Values	Unit
Resistance	11.8	mOhm
Synchronous Inductance	53.1	µH
Back EMF Constant	0.0384	V-s/rad
Stack Length	37.5	mm
Stator Outer Diameter	85	mm
Rotor Outer Diameter	39.2	mm
Air-Gap	0.9	mm
Wire Diameter	2	mm
Series Turns	18	Turns
Residual Flux Density of PM	1.37	Tesla
Coercivity of PM	1030	kA/m

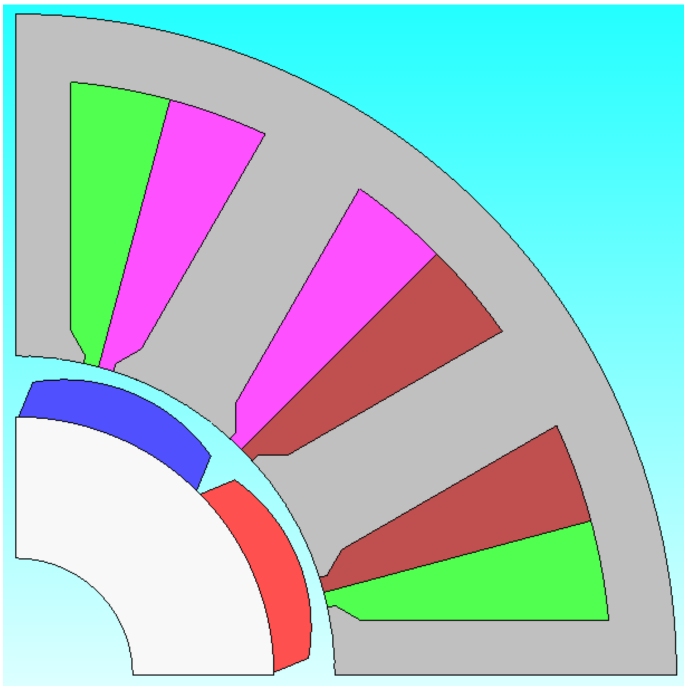

Figure 1. Design base model.

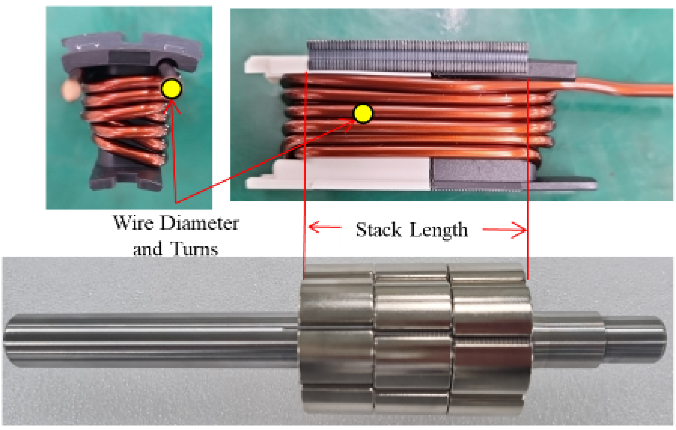

Figure 2. Design variables.

3. Sizing Theories and Procedure

3.1. Magnet Flux Loss

There are several magnetic materials used in the electrical motor. Among them, the NdFeB sintered magnet is suitable for high-power density and compact-size motors due to its excellent magnetic characteristics and is used in various applications. In addition, this magnet requires a coating treatment on the surface to prevent magnetic performance degradation due to damage such as cracks and corrosion, of which there are coating options of various materials and thicknesses, as shown in Table 2.

Table 2. Magnet coating comparison.

Surface Treatment	Thickness [μm]
Phosphate	0.1–0.5
Nickel or Copper	10–20
Zinc	8–20
Epoxy	15–20

According to the research in [18], there is a difference in the magnetic performance of permanent magnets depending on the presence or absence of a coating, as shown in Figure 3. This is because the proportion of raw materials in the magnet itself decreases depending on the coating thickness and the overall size of the magnet, as shown in Figure 4. It would be expected that the thicker the coating, the greater the reduction in the active material at the expense of the thickness of the protective layer of the magnet. Additionally, it can be expected that the smaller the size of the magnet and the shorter the axial length, the greater the magnetic flux loss will be. In the case of motors with high output power, such as vehicle traction motors, the ratio of the coating thickness to the magnet's size is tiny, so this effect can be ignored. However, in the case of an electric power steering (EPS) motor that requires an output of around or less than 1 kW, the magnetic flux loss component due to the thickness of the magnet coating can act as the root cause of errors between the design value and the actual measurement.

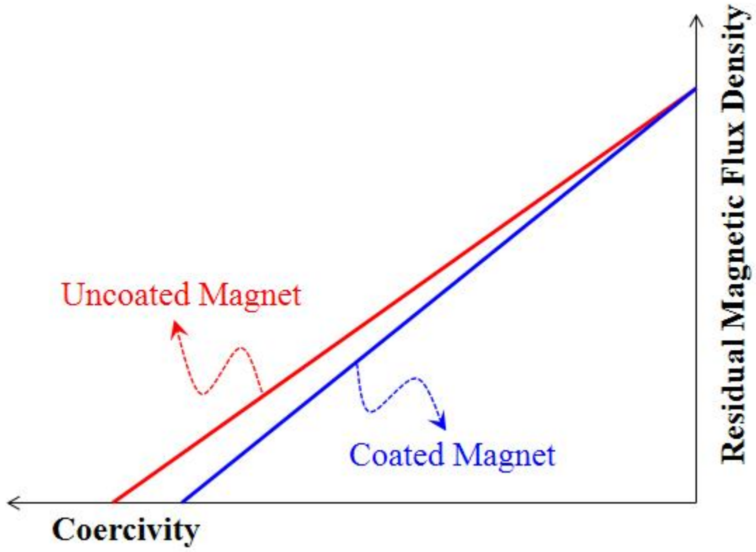

Figure 3. B–H curve comparison between magnets with and without coating on surface.

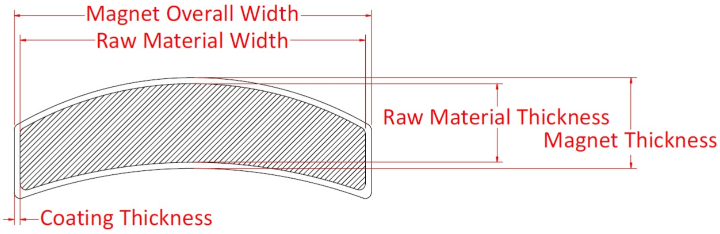

Figure 4. Cross-section of magnet including coating.

Therefore, it is necessary to consider the loss component of the magnetic flux due to the coating thickness of the magnet in the motor design process, especially for low-power electrical motors. In this study, a method for considering the magnetic flux loss was applied by comparing the volume of the magnet's raw material to the total volume of the selected magnet, as shown in Equation (1), to reduce the error between the motor sizing results and the actual test value.

$$L_{p_0} = 1 - \frac{V_r}{V_o} \tag{1}$$

In the equation, L_{p0} is the magnet flux loss, V_r is the raw material volume of the magnet, and V_o is the overall magnet volume, including the coating.

In addition, to improve the productivity of permanent magnets, material loss due to the round shape applied to each corner was considered to be 4% of this design, as shown in Equation (2).

$$L_p = 1 - \frac{V_r}{V_o} + 0.04 \tag{2}$$

In the equation, L_p is the magnet flux loss, including the material loss due to the round edge shape.

Since the two-dimensional shape and dimensions of the reference model have already been designed, the two-dimensional area of the magnet is determined based on the designed value, which is verified using the actual measurement. When calculating the motor sizing, once the coating material and thickness are determined, the area of the magnet's raw material is calculated. By assuming the axial length, the magnetic flux loss for a magnet of the desired length can be calculated using Equation (2).

Figure 5 shows the result of calculating the magnetic loss of the magnet for each coating according to the stack length using the reference model and Equation (2). Here, the coating thickness was considered with the average value in Table 2.

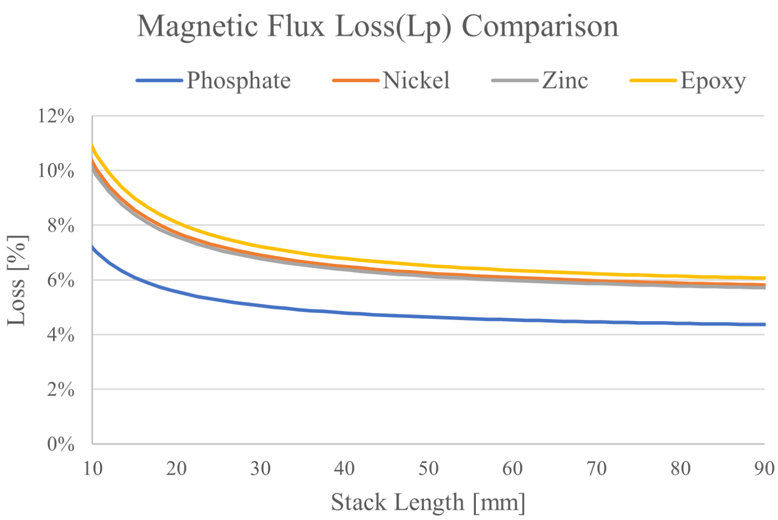

Figure 5. Magnet flux loss calculation results in respect of coating and stack length.

According to these results, it can be seen that the magnetic loss tends to increase as the lamination length decreases and the coating thickness increases, and this was reflected in the sizing process to reduce errors in the test results.

3.2. Back EMF Constant (K_e)

The back electromotive force (back EMF) is an essential indicator of an electric motor's performance. It is calculated as the induced voltage generated per unit speed, as shown in Equation (3), and is determined by many design parameters, as shown in Equation (4) [1].

$$E = K_e \omega \tag{3}$$

In the equation, E is the back EMF voltage, K_e is the back EMF constant, and ω is the angular velocity.

$$K_e = \frac{PZ\Phi}{2\pi a} = \frac{PZBDL_{stk}}{2a} \tag{4}$$

In the equation, P is the pole number, Z denotes the total series turns, Φ is the total magnetic flux per pole, B is the magnetic flux density, D is the diameter of the air gap, L_{stk} is the active stack length, and a is the number of parallel conductors.

According to Equation (4), the back electromotive force is proportional to the number of turns and stack length, which are variables to be used during motor sizing. Therefore, K_{e2} can be calculated easily from the design variables and the magnetic flux loss as defined previously for the reference motor using Equation (5):

$$K_{e2} = K_{e1} \frac{Z_2}{Z_1} \frac{L_{stk2}}{L_{stk1}} \frac{L_{p1}}{L_{p2}} \tag{5}$$

where K_{e1}, Z_1, L_{stk1}, and L_{p1} denote the back EMF constant, number of turns, stack length, and magnetic flux loss of the reference model, respectively. K_{e2}, Z_2, L_{stk2}, and L_{p2} denote the back EMF, number of turns, stack length, and magnetic flux loss of the modification model to be designed, respectively.

The calculation results for K_e obtained by combining the stack length and the number of turns using Equation (5) are shown in Figure 6. This sizing study considered the stack from 10 mm to 90 mm and the winding from 10 to 40 turns.

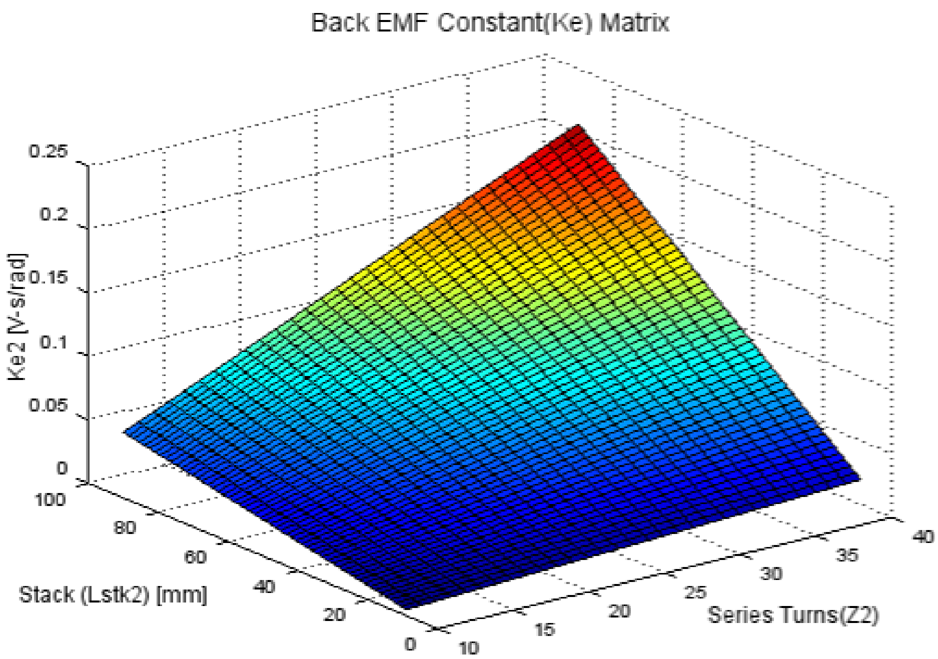

Figure 6. Back EMF constant (Ke) matrix calculated for different turn and stack length combinations.

3.3. Motor Inductance

The motor inductance is a parameter affected by many design variables, such as the intensity of the magnetic flux, number of turns, and length of stacking, as shown in Equation (6) [3].

$$L = \frac{\lambda}{i} = \frac{N\Phi}{i} = \frac{N^2\Phi}{\mathcal{F}} = N^2\mathcal{P} = \mu\frac{N^2 A}{l} \tag{6}$$

where L is the motor inductance, λ is the total magnetic flux linkage, i is the current, N is the total series turns, Φ is the magnetic flux in the coil, $\mathcal{F}$ is the magnetomotive force, $\mathcal{P}$ is the permeance, A is the cross-sectional area, and l is the length of the magnetic circuit.

In the same two-dimensional magnetic circuit, the cross-sectional area A is proportional to the stack length L_{stk}. Therefore, the inductance would be proportional to the stack length and the square of the winding turns. As the ampere-turn condition increases, the inductance may differ from the result obtained using the above Equation (6) due to magnetic saturation in the magnetic circuit. However, to develop an efficient and rapid calculation method in this study, the design was assumed to be under ampere-turn conditions, where magnetic saturation does not occur and the inductance was calculated using the equation of the linear relationship. In this way, the inductance for all combinations of turns and stack lengths can be calculated using Equation (7), as shown in Figure 7.

$$L_{s2} = L_{s1}\left(\frac{Z_2}{Z_1}\right)^2 \frac{L_{stk2}}{L_{stk1}} \frac{L_{p1}}{L_{p2}} \tag{7}$$

where L_{s1} and L_{s2} denote the inductance of the reference and the modification model to be designed, respectively.

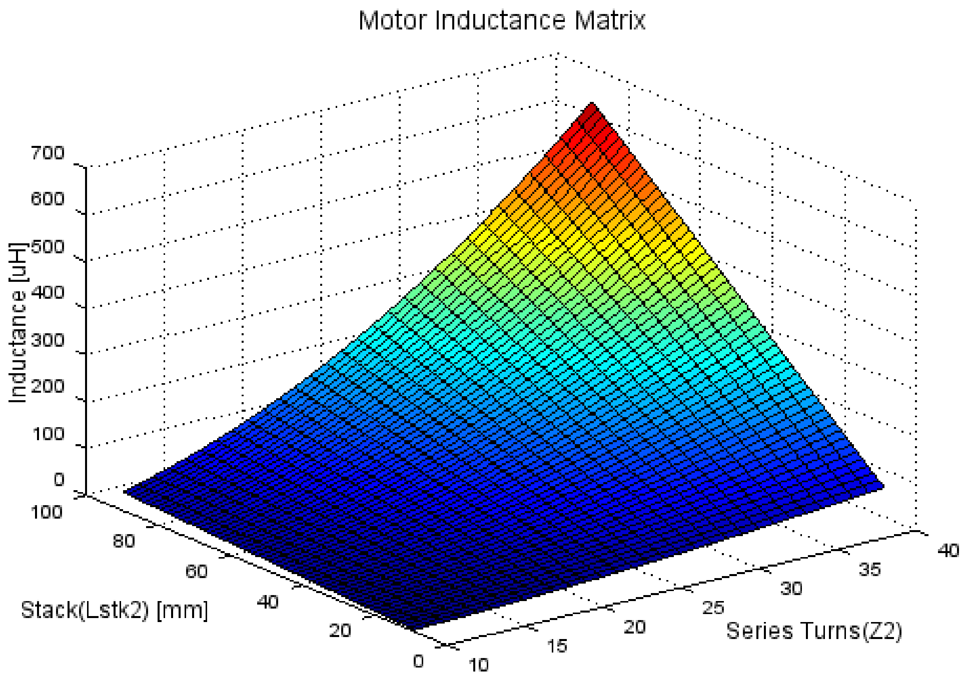

Figure 7. Inductance matrix calculated using different turn and stack length combinations.

3.4. Current Density

The current density of a motor is related to the coil's durability and the motor's temperature characteristics. The lower the current density, the better the motor characteristics, but the size increases, so selecting an appropriate current density level is necessary.

Most electric power steering motors have a completely sealed structure, and due to the instantaneous operation behavior, they use a cooling method via natural convection without an additional cooling device. Therefore, selecting a current density level in the range 15 to 25 Arms/mm^2 at the maximum current condition is generally appropriate for this design, which operates in an instantaneous condition.

The coil diameter of the motor to be designed can be determined using the input current and the number of parallel circuits, as shown in Equations (8) and (9) below.

$$J_c = \frac{\frac{I_a}{a}}{\frac{\pi D_c{}^2}{4}} = \frac{4I_a}{\pi a D_c{}^2} \tag{8}$$

Here, J_c is the current density, I_a is the input current, a is the parallel circuit, and D_c is the coil diameter.

$$D_c = \sqrt{\frac{4I_a}{J_c \pi a}} \tag{9}$$

Figure 8 below shows the current density calculation result according to the coil diameter with two strands at a 100 A input current condition.

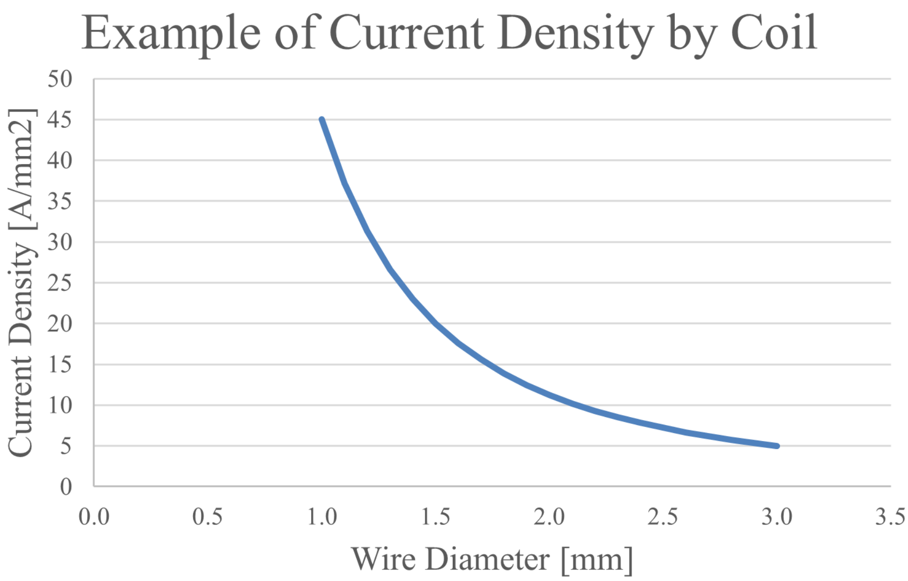

Figure 8. Current density calculation result for different wire diameters at 100 A.

3.5. Winding Feasibility Study

Since the two-dimensional shape of the reference model has already been defined, it is possible to predict the maximum number of turns that can be wound using the actual drawing, as shown in Figure 9. It is advisable to consider the outer coil diameter, including the insulation coating layers and slot insulator thickness in the slots, to minimize differences from the actual product, as shown in the figure.

In this way, it is possible to create a winding capability database of the reference model for a wide range of coil diameters, as shown in Figure 10. The results show the winding feasibility from 1.0 mm to 3.0 mm of the diameter as the condition of the same slot area in this reference model.

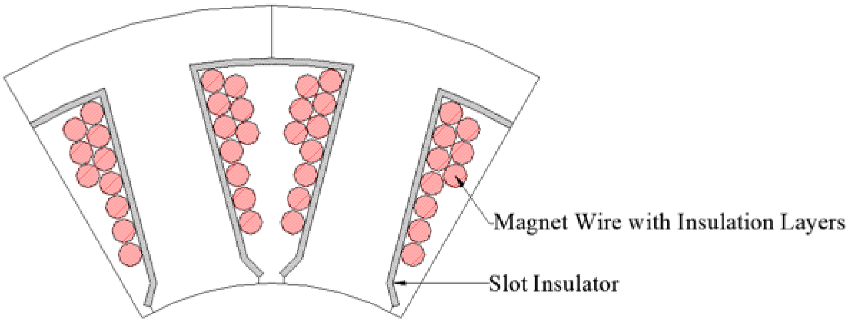

Figure 9. Example of winding feasibility study using drawing.

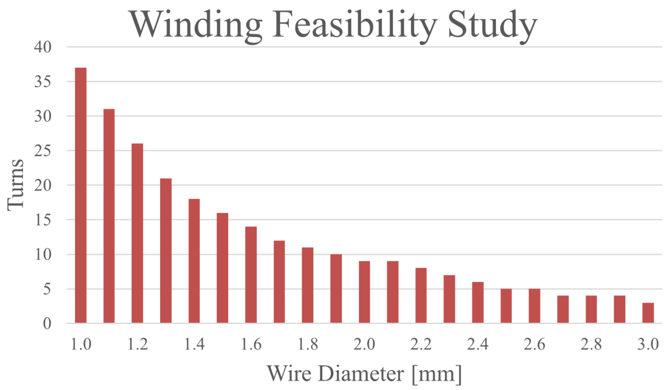

Figure 10. Winding feasibility study: max winding turn by wire diameter.

3.6. Resistance

The general formula for electrical resistance is as follows.

$$R = \rho_c \frac{l_c}{A_c} \tag{10}$$

where R is the motor resistance, ρ_c is the resistivity of the coil, l_c is the total length of the coil, and A_c is the cross-sectional area of the coil.

The length of the conductor can be calculated using Equation (11) to Equation (17) and the parameters defined in Figure 11.

$$R_c = \frac{D_c}{2} = \frac{D_{so} - D_{si}}{2} + D_{si} \tag{11}$$

In the equation, R_c and D_c are the radius and diameter center dimension of the coil wound on the stator, respectively, and D_{so} and D_{si} are the outer and inner diameters of the stator core, respectively, as defined in Figure 11.

All the parameters defined in the figure can be calculated as follows.

$$\theta_1 = \frac{360}{Q} \tag{12}$$

where Q is the number of stator slots and θ_1 is the one slot angle.

$$\theta_2 = \arcsin(\frac{W_{st}}{2R_c}) \tag{13}$$

where W_{st} is the tooth width of the stator core and θ_2 is the half-slot coil pitch angle.

$$\theta_3 = \frac{\theta_1}{2} - \theta_2 \tag{14}$$

$$\theta_4 = \theta_2 + \frac{\theta_3}{2} \tag{15}$$

$$\tau_s = 2R_c \sin\theta_4 \tag{16}$$

where τ_s is the one coil pitch.

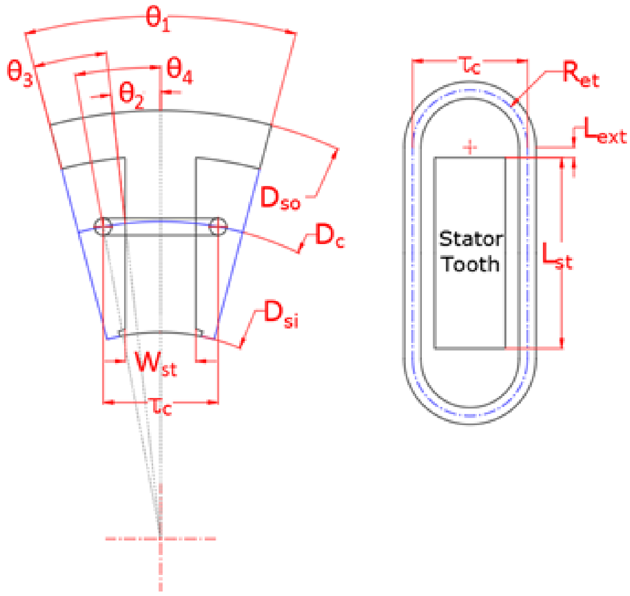

Figure 11. Parameters for calculating winding resistance.

In addition, L_{ext}, defined in Figure 11, is a length depending on the thickness of the slot insulator. Assuming that the coil at the end turn area is formed in a semicircle as large as the coil pitch dimension, the coil length per turn l_{c1} and resistance per turn R_{c1} are as follows.

$$l_{c1} = 2\left(L_{st} + \frac{\pi\tau_c}{2} + L_{ext}\right) \tag{17}$$

$$R_{c1} = \rho_c \frac{l_{c1}}{A_c} \tag{18}$$

Using the given number of turns N_{ph} and parallel circuits a, the phase resistance can be calculated as shown in Equation (19). Also, using copper's resistance temperature coefficient α_c, changes in the resistance value at a sizing temperature condition (t degrees) can be calculated using Equation (20).

$$R_{ph} = R_{c1}\frac{N_{ph}}{a} \tag{19}$$

$$R_{ph}(t) = R_{ph}(1 + \alpha_c(t - RT)) \tag{20}$$

In the equation, α_c is the temperature coefficient of copper calculated as 3.93×10^{-8} Ω m; t is the sizing temperature given by the requirement; and RT is room temperature.

In this sizing technique, only the coil diameter, number of turns, and lamination length are design variables, and by using Equations (17)–(20), the resistance values for all cases under different conditions can be calculated.

3.7. Torque Constant Saturation, Torque Ripple, and Demagnetization

The torque constant (K_T) is the torque per unit current and, like the back electromotive force constant (K_e), is a parameter that represents the unique characteristics of the electric motor. Kt decreases due to the magnetic saturation effect of the magnetic circuit in the motor as the current increases. Due to this magnetic saturation phenomenon, the term Kt saturation is used to refer to the change in K_T.

In a sinusoidal drive three-phase motor, the back EMF constant (K_e) and torque constant (K_T) have the following specific relationship [1].

$$K_T = \frac{\sqrt{3}}{2} K_e. \tag{21}$$

Here, the unit of the back EMF constant (K_e) is Vll-pk/rad/s and the torque constant (K_T) is Nm/Apk.

The relationship in Equation (21) shows the ideal condition established with no effect from magnetic saturation or temperature. From this relationship, the ratio of the Kt value between the model at no load and at a specific load current condition can be defined as in Equation (22) below.

$$K_s = 1 - \frac{K_{T1}}{K_{T0}} \tag{22}$$

where K_s is the saturation ratio of the torque constant compared between a torque constant K_{T1} at a specific current condition and the torque constant K_{T0} without a current condition, as defined from Equation (21).

When the saturation of the torque constant increases, the torque value generated from the motor decreases compared to the reference model and torque ripple tends to increase.

These non-linear characteristics must be calculated in advance for each ampere-turn condition using the reference model via FEM analysis S/W, which allows for precise calculation. In this way, when an urgent sizing request is made by a customer at any time, the results of the non-linear characteristics for all ampere turns that have been reviewed in advance can be used as a lookup table to increase prediction precision and enable rapid response without performing FEM S/W analysis.

The demagnetization of PMSM is another characteristic showing a nonlinear trend due to the demagnetization curve having a knee point at a particular coercivity condition.

In this study, the nonlinear analysis was performed from 50 to 5000 ampere turns and the non-linearity data on Kt, torque ripple, and demagnetization were secured in advance to build a database as shown in Figures 12 and 13.

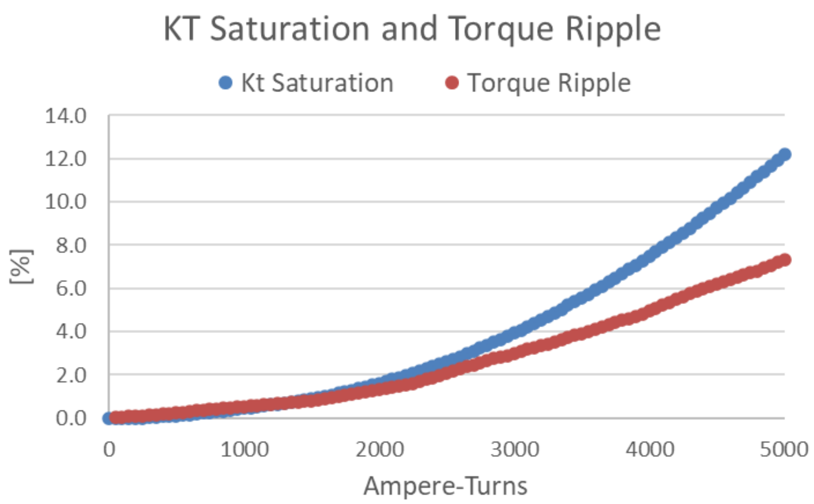

Figure 12. Kt and torque ripple by ampere turns.

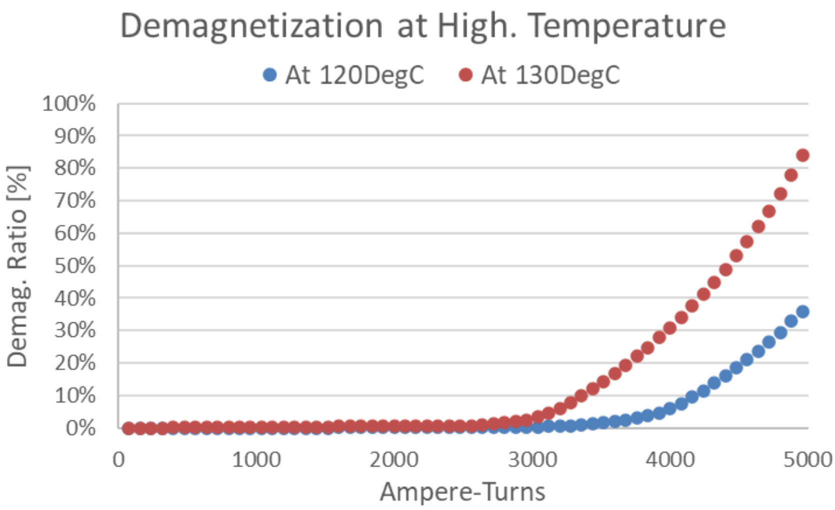

Figure 13. Demagnetization by ampere turns and temperature.

3.8. Torque–Speed Performance

The design of an electric motor involves finding parameters such as magnetic flux, inductance, and resistance that satisfy the voltage equation and torque equation expressed in Equations (23) and (24) [19,20].

$$T = P_n\{\Phi_a i_q + (L_d - L_q)i_d i_q\} = P_n\left\{\Phi_a i_a \cos\beta + \frac{1}{2}(L_q - L_d)i_a^2 \sin 2\beta\right\} \tag{23}$$

$$(L_d i_d + \Phi_a)^2 + (L_q i_q)^2 = \left(\frac{V_{om}}{\omega}\right)^2 \tag{24}$$

In the equation, T is torque; P_n is the pole pair number of the magnet; Φ_a is magnetic flux linkage; β is the current angle; L_d and L_q are the d- and q-axis inductance, respectively; i_d and i_q are the d- and q-axis current, respectively; i_a is the input current; V_{om} is voltage; and ω is the angular velocity.

Equation (23) will be more straightforward because of the same L_d and L_q in SPMSM.

The torque–speed characteristic is one of the final performances determined by fundamental parameters such as the resistance, inductance, and magnetic flux linkage of an electric motor, and there can be countless combinations of these parameters to satisfy the performance. Among these results, the optimal decision as an electric motor designer is to select the smallest stack length electric motor in consideration of the price.

Using the three parameters of back EMF constant (Ke), resistance, and inductance, which are the fundamental parameters of the motor described previously, the required torque and speed characteristics can be calculated within the given constraints such as input voltage and current limits.

The magnetic flux linkage Φ_a can be obtained using Equations (25) and (26) [1,3,4].

$$E_0 = \frac{K_{e2}}{\omega} \tag{25}$$

$$\Phi_a = \frac{E_0}{\omega_{em}} \tag{26}$$

where E_0 is the back EMF without load current, K_{e2} is the calculated value from Equation (5), and ω is the mechanical rotation velocity. It has a 1/pole pair relationship with the electrical rotation velocity ω_{em}.

In Equations (23) and (25), the pole pair (P_n) has been defined already from the reference design. The voltage (V_{om}) can be limited as shown in Equation (27) by the phase resistance (R_{ph}), calculated in Section 3.5, and the given input current (I_a), from the requirement.

$$V_{om} = V_{ph} - I_a R_{ph} \quad (27)$$

Moreover, the inductance (L_d and L_q) and the magnetic flux linkage (Φ_a) were found in the previous procedures.

Therefore, the torque and the rotation velocity in Equations (23) and (25) can be calculated by chaining the current angle (β).

3.9. Sizing Procedure

The procedure for the sizing technique proposed in this paper is shown in Figure 14. First, it is necessary to define the target values for the performance parameters, such as K_e, resistance, inductance, etc., of the electric motor to be designed. Then, we determine the magnet coating specifications to be applied to the motor, calculate the magnetic flux loss components of the magnets as described in Section 3.1, and calculate the Ke matrix and inductance matrix for the stack length and series turns, respectively, based on the reference model as explained in Section 3.2 to Section 3.3. Next, the stack length for each turn that satisfies the requirements is selected from the calculated K_e and inductance results.

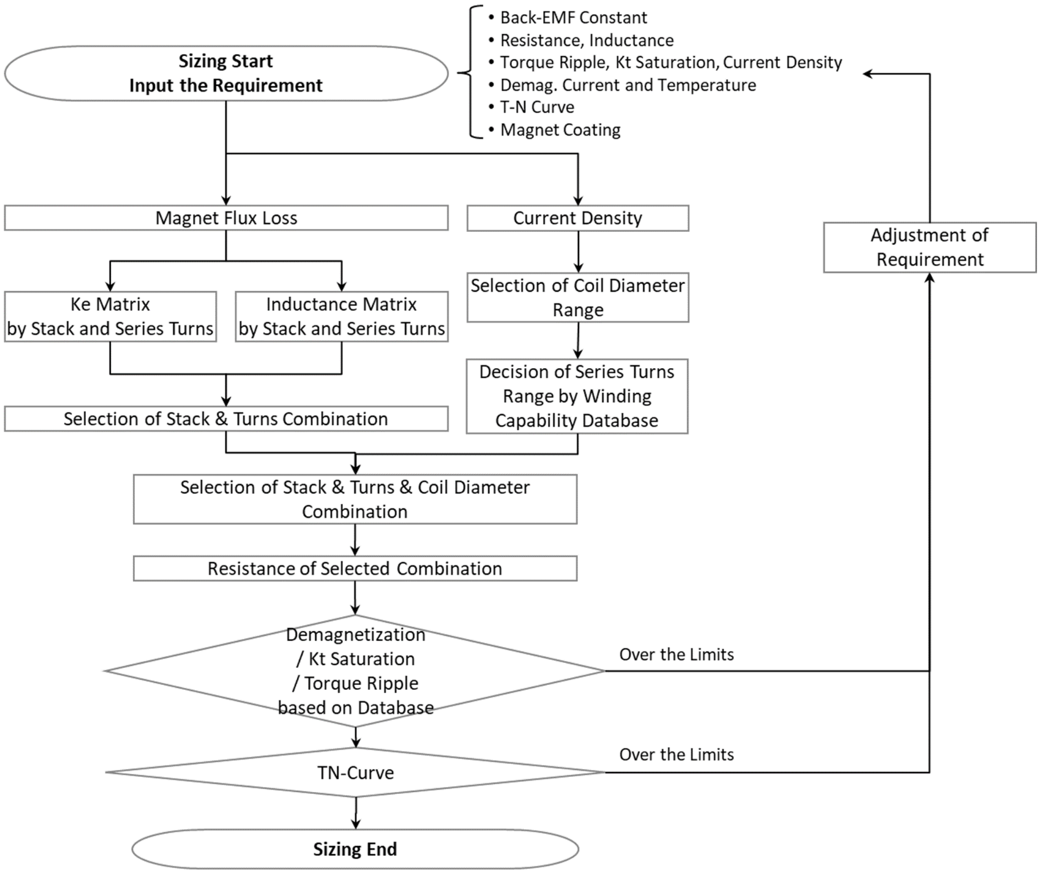

Figure 14. Process flow of motor sizing.

The current density of the coil is calculated using the given current value and a coil diameter with a current density that meets the requirements is selected as described in Section 3.4. The maximum number of turns is determined using the winding capability database of the base model, as explained in Section 3.5.

The next step is to calculate resistance values based on Section 3.6 for combinations of wire diameters, number of turns, and stack lengths that satisfy K_e, inductance, and current density. These combinations are checked using the database to see if nonlinear characteristics such as torque ripple and demagnetization are satisfied, as explained in Section 3.7. The torque–speed (T–N) characteristic calculation is performed using the determined parameters if all conditions are satisfied. Otherwise, the requirements need to be adjusted as described in Section 3.8.

The results can be checked at a glance as soon as the requirements are input because none of these processes require a separate nonlinear calculation process using FEM S/W or any additional calculation.

4. Verification

The proposed sizing method in this paper was verified by comparing with FEM analysis and the test results using actual samples.

4.1. Study Case 1

The requirements for the first study case are summarized in Table 3 and Figure 15. The given conditions for the sizing performance are 6.6 VrmsLL, 109 Arms, and 23 °C.

Table 3. Requirements for Study Case 1 Motor.

Parameters	Values	Unit
Resistance	Max 14	mOhm
Synchronous Inductance	57–63	µH
Back EMF Constant (*Ke*)	0.04–0.044	V-s/rad
Max Phase Current	109	Arms
Current Density	10–25	A/mm
Demag. Current	167.4	A
Demag. Temperature	130	°C
Demag. Ratio	Max 5	%
Kt Saturation	Max 5	%
Torque Ripple	Max 4	%
Rated Torque @30 rpm	Min 5	Nm

The sizing result for the suggested motor sizing technique according to the sizing process described in Figure 14 is summarized in Table 4 and Figure 16.

This result was compared to the FEM analysis shown in Figure 17 and the sample test. As a comparison, the proposed sizing method shows a reasonable deviation from the FEM analysis and the actual test result, as marked with parentheses in the table. The values in parentheses denote the differences compared to the values obtained from the sizing results.

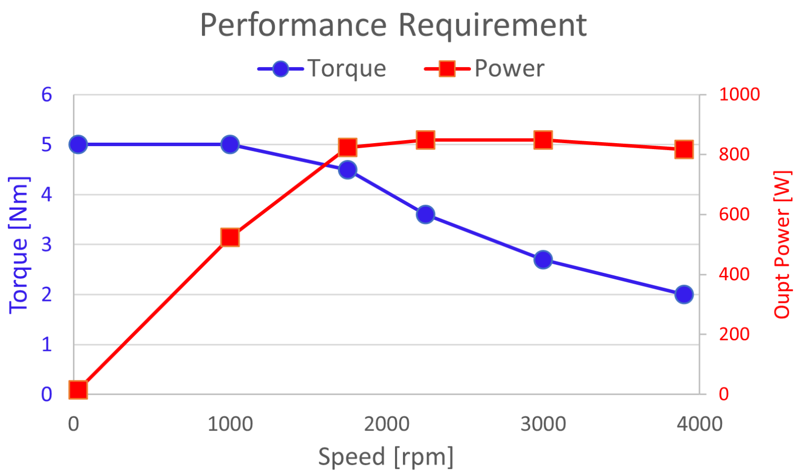

Figure 15. Performance requirement for Study Case 1.

Table 4. Sizing results and comparison for Study Case 1 motor.

Parameters	Unit	Sizing Result	FEM Analysis	Test Result
Wire Diameter	mm	2.0	2.0	2.0
Series Turns	Turns	18	18	18
Stack Length	mm	40.5	40.5	40.5
Resistance	mOhm	11.32	11.32	11.9 (5%)
Inductance	µH	57.4	58.5 (2%)	59 (3%)
Ke	V-s/rad	0.0416	0.0415 (0%)	0.0415 (0%)
Demag. Ratio	%	3.37	3.5 (4%)	3.21 (5%)
Torque Ripple	%	2.57	2.31 (10%)	2.91 (13%)
Torque @30 rpm	Nm	5.26	5.13 (2%)	5.18 (2%)
Torque @3900 rpm	Nm	2.05	2.29 (12%)	2.23 (9%)
Total Calculation Time	-	<1 s	around 1.5 h	-

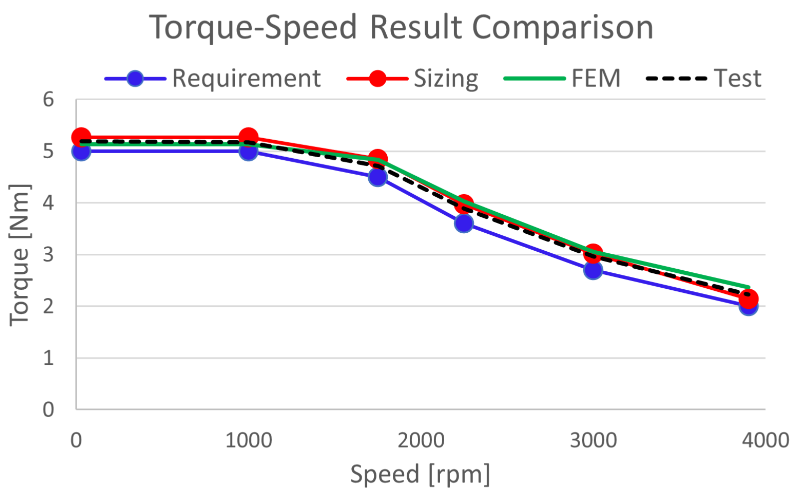

Figure 16. Torque–speed performance comparison for Study Case 1.

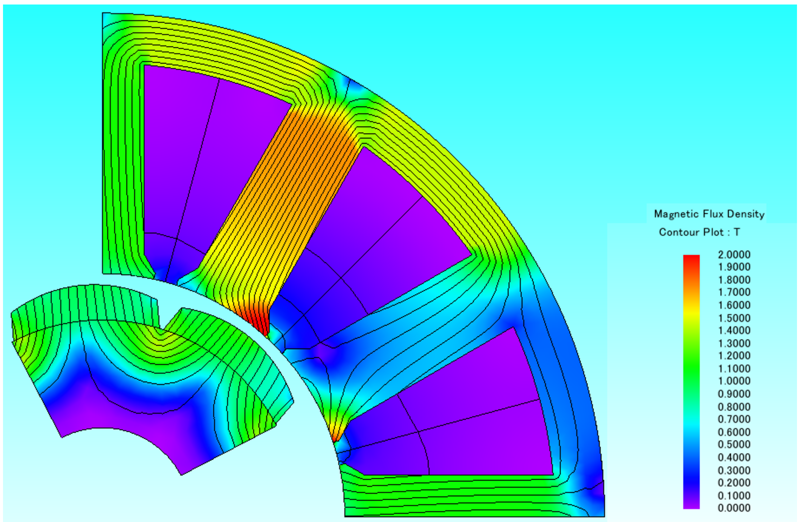

Figure 17. Magnetic flux line and density distribution for FEM analysis model at 154 Apk, Current Angle 0, and Elec.Deg.

4.2. Study Case 2

Table 5 and Figure 18 summarize the requirements for the second study case. The given conditions for the sizing performance are 6.0 VrmsLL, 113 Arms, and 23 DegC.

Table 5. Requirements for Study Case 2 motor.

Parameters	Values	Unit
Resistance	Max 18	mOhm
Synchronous Inductance	80–90	µH
Back EMF Constant (*Ke*)	0.067–0.074	V-s/rad
Max Phase Current	103	Arms
Current Density	10–25	A/mm
Demag. Current	176	A
Demag. Temperature	130	Deg.C
Demag. Ratio	Max 5	%
Kt Saturation	Max 5	%
Torque Ripple	Max 4	%
Rated Torque @30 rpm	Min 8.7	Nm

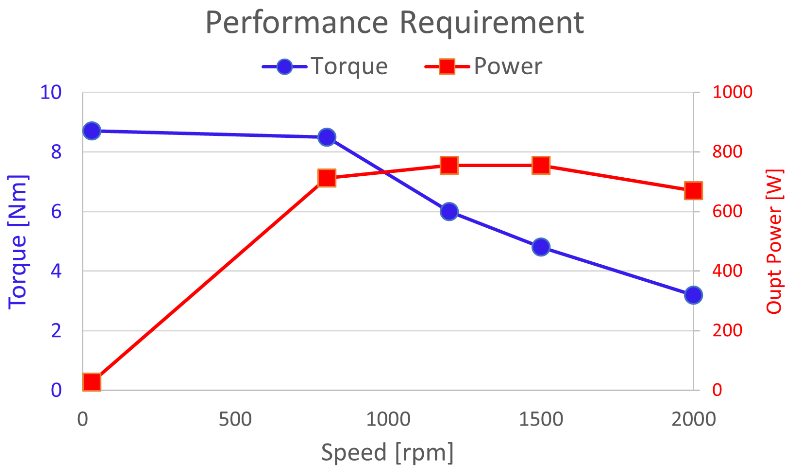

Figure 18. Performance Requirement for Study Case 2.

The sizing results for the second study case are similar to the FEM analysis and actual test results except for the torque ripple and demagnetization ratio, as shown in Table 6 and Figure 19. There are considerable deviations compared with the percentage unit for the demag. ratio and torque ripple comparison, but they are not large differences compared with the absolute values.

Table 6. Sizing results and comparison for Study Case 2 motor.

Parameters	Unit	Sizing Result	FEM Analysis	Test Result
Wire Diameter	mm	2.2	2.2	2.2
Series Turns	Turns	16	16	16
Stack Length	mm	73.5	73.5	73.5
Resistance	mOhm	15.1	15.1 (0%)	15.5 (5%)
Inductance	µH	83.8	82.6 (1%)	81 (3%)
Ke	V-s/rad	0.0675	0.0675 (0%)	0.0675 (0%)
Demag. Ratio	%	1.58	1.4 (11%)	1.2 (23%)
Torque Ripple	%	2.2	2.4 (9%)	2.7 (23%)
Torque @30 rpm	Nm	8.93	8.85 (1%)	8.91 (0%)
Torque @2000 rpm	Nm	3.34	3.6 (8%)	3.71 (11%)
Total Calculation Time	-	<1 s	around 1.5 h	-

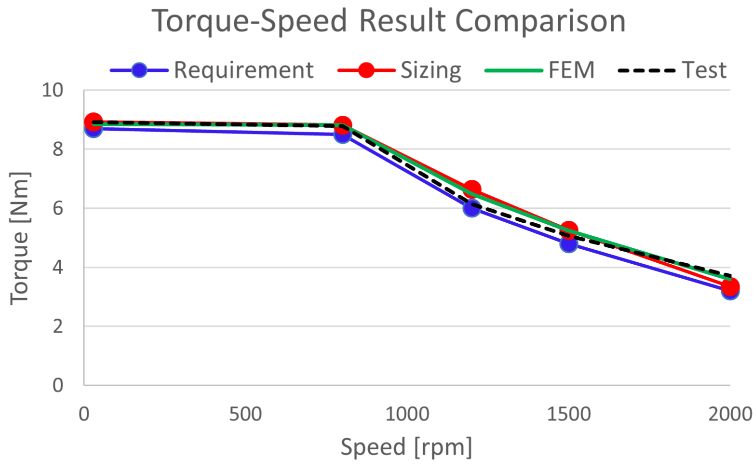

Figure 19. Torque–speed performance comparison for Study Case 2.

Figure 20 shows the test samples for the rotor, stator, and motor assembly to be used for this study.

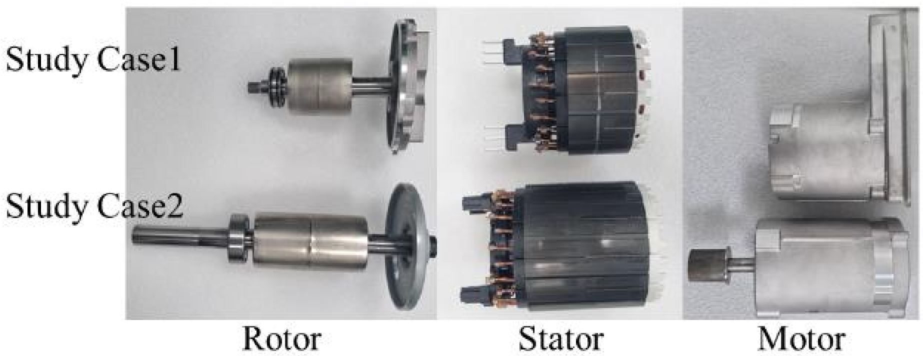

Figure 20. Test samples for Study Case 1 and Study Case 2.

As shown by the verification results for two kinds of motor specification, the proposed sizing technique has good fidelity to the FEM analysis and test results using the test samples even though it does not need a long calculation time, unlike expensive FEM S/W.

5. Conclusions

In this paper, we proposed a practical and rapid sizing method for existing platform motors that could reduce production costs using key components, such as the rotor core and stator core. The motor parameters to be designed are calculated using the equations and based on the parameters of the reference model. The magnetic flux loss due to the magnet coating is considered to increase the accuracy of the results. Nonlinear characteristics, such as torque ripple and demagnetization, are reflected by setting up a database via accurate FEM results in advance to enhance the fidelity of the results. Nonlinear calculation via FEM is required only once when setting up the database for the reference model. This method has been verified using two study case specifications, and the proposed sizing results compare well to the FEM and test results.

This method will help researchers create designs using existing products in a short time under the condition of no changes to the two-dimensional shape and material of the motor. The method does not need a certain level of experience for the motor designer and does not involve using expensive FEM S/W.

Moreover, it can be applied regardless of the type and configuration of the motor under the premise that only the stack length, number of turns, and coil diameter change from the reference model.

For future works, the model needs to be studied further to improve the calculation accuracy for non-linear parameters such as torque ripple, demagnetization, and inductance, which could be affected easily by magnetic saturation.

Author Contributions: Conceptualization, Y.-C.K. and J.-H.H.; methodology, Y.-C.K. and J.-H.H.; software, Y.-C.K.; validation, Y.-C.K.; formal analysis, Y.-C.K. and J.-H.H.; investigation, Y.-C.K. and J.-H.H.; resources, Y.-C.K.; data curation, Y.-C.K.; writing—original draft preparation, Y.-C.K.; writing—review and editing, Y.-C.K.; visualization, Y.-C.K.; supervision, J.L.; project administration, J.L. All authors have read and agreed to the published version of the manuscript.

Funding: This research was supported by the Nano & Material Technology Development Program through the National Research Foundation of Korea (NRF) funded by Ministry of Science and ICT (NRF-2020M3H4A3106183).

Data Availability Statement: Data is contained within the article.

Conflicts of Interest: The authors declare no conflict of interest.

Abbreviations

The following abbreviations are used in this manuscript:

Demag.	Demagnetization
EPS	Electric power steering
FEM	Finite element method
NdFeB	Neodymium iron boron
PM	Permanent magnet
PMSM	Permanent magnet synchronous motor
SPMSM	Surface permanent magnet synchronous motor
S/W	Software

References

1. Hendershot, J.R.; Miller, T.J.E. Design of Brushless Permanent-Magnet Machines. In *Motor Design Books LLC* , 2nd ed.; Clarendon Pr: Oxford, UK , 2010.
2. Islam, R.; Husain, I.; Fardoun, A.; McLaughlin, K. Permanent Magnet Synchronous Motor Magnet Designs with Skewing for Torque Ripple and Cogging Torque Reduction. *IEEE Trans.* **2007**, *7*, 1552–1559.
3. Thomas, A. *Lipo, Introduction to AC Machine Design*; IEEE Press Wiley: Piscataway, NJ, USA, 2017.
4. Jacek, F.G. *Permanent Magnet Motor Technology*, 3rd ed.; CRC Press: Boca Raton, FL, USA, 2010.
5. Hamdi, E.S. *Design of Small Electrial Machines*; Wiley: Hoboken, NJ, USA, 1994.
6. Fei, W.; Zhu, Z.Q. Comparison of Cogging Torque Reduction in Permanent Magnet Brushless Machines by Conventional and Herringbone Skewing Techniques. *IEEE Trans. Energy Convers.* **2013**, *28*, 664–674. [CrossRef]
7. Islam, M.S.; Mir, S.; Sebastian, T. Issues in Reduction the Cogging Torque of Mass-Produced Permanent-Magnet Brushless DC Motor. *IEEE Trans. Ind. Appl.* **2004**, *40*, 813–820. [CrossRef]
8. Hanselman, D.C. Effect pf skew, pole count and slot count on brushless motor radial force, cogging torque and back emf. *IEEE Proc.-Electr. Power Appl.* **1997**, *144*, 325–330. [CrossRef]
9. Wang, X.; Yang, W.; Fu, D. Study of cogging torque in surface-mounted permanent magnet motors with energy method. *J. Magn. Magn. Mater.* **2003**, *267*, 80–85. [CrossRef]
10. Bianchi, N.; Blolgnani, S. Design techniques for reducing cogging torque in surface-mounted PM motors. *IEEE Trans. Ind. Appl.* **2002**, *38*, 1259–1265. [CrossRef]
11. Hwang, S.M.; Eom, J.B.; Jung, Y.-O.; Lee, D.-W.; Kang, B.-S. Various design techniques to reduce cogging torque by controlling energy variation in permanent magnet motors. *IEEE Trans. Magn.* **2001**, *37 Pt 1*, 2806–2809. [CrossRef]
12. McKerracher, C. *Electric Vehicle Outlook 2023, September 2017*; BloombergNEF: London, UK, 2017.
13. Jung, T.C. A Study on IPMSM Basic Design Using per-Unit Design Methods and Construction of Non-Linear Data Set. Ph.D. Thesis, Hanyang University, Seoul, Republic of Korea, 2016.
14. Harrer, M.; Pfeffer, P. *Steering Handbook*; Springer: Berlin/Heidelberg, Germany, 2016.
15. Yang, H.; Ademi, S.; Paredes, J.; McMahon, R.A. Comparative Study of Motor Typologies for Electric Power Steering. In Proceedings of the 2021 IEEE Workshop on Electrical Mechanics Design, Control and Diagnoosis (WEMDCD), Online, 8–9 April 2021; pp. 40–45.
16. Yuga, T.; Hironoshi, M.; Yusuke, F.; Akira, C. Reduction of Torque Ripple and Radial Force harmonics in Consequent-Pole Permanent Magnet Motor for electric Power Steering Application. In Proceedings of the 2022 25th International Conference on Electrical Machines and Systems (ICEMS), Chiang Mai, Thailand, 29 November–2 December 2022.

17. Won, Y.J.; Kim, J.H.; Park, S.H.; Lee, J.H. Transfer Learning-Based Design Method for Cogging Torque Reduction in PMSM with Step-Skew Considering 3-D Leakage Flux. *Proc. IEEE Trans. Magn.* **2023**, *59*, 8204905. [CrossRef]
18. Liu, Y. Discussion on several principal problems aroused from measuring high performance permanent magnetic materials. *Int. J. Appl. Electromagn. Mech.* **2017**, *55*, 453–479. [CrossRef]
19. Lee, J.; Kim, K.C.; Ahn, J.S.; Won, S.H. *Design and Control of IPMSM, Intervision, Republic of Korea*; Intervision: Daegu, Republic of Korea, 2007; pp. 10–35.
20. Morimoto, S. *Design, Analysis, and Control of Interior PM Synchronous Machines*, 3rd ed.; IEEE Industry Applications Society Annual Meeting Seattle: Seattle, WA, USA, 2004; Chapter 8, pp. 8.1–8.8.